Construction and Building Materials 525 (2026) 146416

Contents lists available at ScienceDirect

Construction and Building Materials

journal homepage: www.elsevier.com/locate/conbuildmat

Impact of wind turbine blade waste fiber size on the properties of mortar: From material characteristics to performance

Tao Liu *, Charilaos Paraskevoulakos, Diego J. De Souza, Wolfgang Kunther, Ana Teresa Lima

Construction Materials and Durability, Department of Environmental and Resource Engineering, Technical University of Denmark, 2800 Kgs., Lyngby, Denmark

ARTICLE INFO

Keywords:
Wind turbine blade waste
Fiber size
Fiber reinforcement
Reactivity
XCT
SEM-EDS
Alkali silica reaction

ABSTRACT

This study investigates the use of wind turbine blade (WTB) waste in mortar, with emphasis on how particle size affects hydration, mechanical performance, and alkali-silica reaction (ASR) expansion. Mechanically shredded WTB waste, composed mainly of glass fiber and epoxy resin, is used in mortar in different particle sizes: from 0.063 mm to larger than 8 mm. Experiments assessed the physical and chemical interactions of the different WTB waste fiber sizes with the cementitious matrix using isothermal calorimetry, X-ray diffraction, and scanning electron microscopy. Flexural and compressive strength, as well as ASR expansion of all the WTB waste-reinforced mortar were also determined. The results show that smaller WTB fractions (0.063–2 mm) contained more exposed glass surfaces, exhibited higher reactivity, and improved compressive strength while reducing porosity. However, these finer fractions also caused faster and greater ASR expansion. In contrast, larger WTB fractions (>8 mm), which more often retained epoxy resin on the fiber surface, showed lower early ASR expansion but introduced more defects and higher porosity, resulting in reduced compressive strength. The intermediate fraction (2–8 mm) displayed mixed powder-like and fiber-like behavior. WTB size strongly governs the balance between mechanical performance and ASR-related durability, showing that this waste stream can only be incorporated safely when its particle-size-dependent effects are carefully considered.

1. Introduction

Over the past two decades, wind energy has emerged as key technology for the green energy transition, experiencing substantial growth in installed capacity [1] – and with it, the rise of wind turbine blade (WTB) waste also rises [2]. Utilizing WTB waste in cement and concrete matrices offers potential solutions for the growing global problem of WTB disposal [3–6]. This approach mitigates adverse environmental consequences associated with incineration and landfilling, while also reducing the expenses incurred by producers and suppliers of WTB due to fewer fines for landfilling. Previous studies have identified three primary methods for incorporating WTB waste into cement/concrete matrix: fiber reinforcement, aggregate replacement, and cement replacement [7]. Given that the recycling process of WTB typically yields fiber-like products after mechanical shredding [8,9], these fibers can be utilized as reinforcement in cementitious matrices. However, while previous studies have explored the incorporation of WTB waste in concrete matrices [3,7], this study uniquely investigates the influence of WTB fiber size on alkali-silica reaction (ASR) mitigation, a previously underexplored area.

Even though incorporating WTB waste into concrete may enhance its structural integrity and physical characteristics [10,11], its durability properties have not been thoroughly studied in the existing literature. This is especially true when considering the potential contribution of partially reactive SiO_2 from the glass fiber included in WTB waste becoming reactants to alkali-silica reaction (ASR) in laboratory conditions [12]. ASR is a deleterious process in concrete, leading to significant structural issues. This reaction occurs between alkali and hydroxide ions (Na^+, K^+, and OH^-) in the concrete's pore solution and poorly crystalline and therefore reactive silica minerals present in aggregates (e.g. opal, flint) [13–16]. The interaction produces expansive reaction products (the so-called ASR-gel) that induce internal pressure, resulting in cracking of both aggregates and the surrounding cement paste [16]. These cracks compromise the concrete's integrity and facilitate the ingress of other harmful agents, potentially triggering further degradation mechanisms such as sulfate attack, chloride penetration,

* Corresponding author.
E-mail address: taliu@dtu.dk (T. Liu).

https://doi.org/10.1016/j.conbuildmat.2026.146416
Received 12 February 2026; Received in revised form 14 April 2026; Accepted 17 April 2026
Available online 20 April 2026

freeze-thaw damage, and accelerated carbonation. Effective preventive measures against ASR expansion and damage include using non-reactive aggregates, low-alkali binders, and controlling the moisture content in the concrete [17]. However, these solutions are not always feasible, particularly due to the limited availability of non-reactive aggregates. In this context, using fiber reinforcement in a cementitious matrix has proven to be an effective way to mitigate the harmful effects of ASR [18–20].

The mechanical shredding process of WTB waste yields fiber-like products, offering the potential to be used to reinforce the cementitious matrix. The WTB waste fiber contains fibers of different sizes (different widths and different length) after the shredding process. The shredding process can be easily scaled up for industrial applications, making it a viable solution for large-scale concrete usage. Fibers can mitigate the expansion and shrinkage of the matrix by providing additional reinforcement, facilitating cracking control, and toughness of the brittle composite material [21–23]. In general, WTB waste consists of two major components: glass fiber and epoxy resin, although some blade waste may contain also other fibers and resins [24,25]. Previous studies show that glass fiber may react with the pore solution of the cementitious matrix, forming Ca/Na-silicate gels and lead to increased expansion [26]. The presence of epoxy resin in WTB waste fiber may contribute to a decrease of the matrix expansion due to reduced ASR gel formation, because the resin is tightly bound to the glass fiber, enhancing its alkaline resistance in the cementitious matrix [27].

More specifically, WTB waste is a composite material with a high content of organic molecules in the epoxy, and inorganic mineralogical profiles (main oxides are SiO_2, CaO, and Al_2O_3) similar to construction materials. The high silicate, aluminum, and calcium content (from glass fiber) in WTB waste react potentially with the pore solution in the cementitious matrix. Shi et al. [28] reported that waste glass (with particle size of 40–700 μm) exhibited very high pozzolanic activity. Similarly, the glass fiber in WTB waste may be reactive. The dissolution process of waste glass under an alkaline environment has been presented in a previous study [29]. The waste glass contributed to more dissolution of Ca and Al, into the pore solution of the cement matrix. Therefore, it is important to assess if epoxy resin can reduce the reactivity of the glass component of WTB waste in cementitiopus systems.

This study focuses on understanding the effect of different sizes of WTB waste fiber on their contribution as supplementary cementitious materials and its effectiveness in reducing ASR-related expansion of the reinforced mortars. The impact of different fiber sizes on the hydration process and the ASR expansion of the matrix were studied. The role of fiber size in affecting hydration and durability remains unclear. Smaller fibers may interact differently with the matrix compared to larger ones, potentially influencing both the chemical reactions and mechanical properties.

The experiments in this study have been conducted in cementitious materials containing WTB waste fibers of different sizes to answer the main hypothesis:

Hypothesis 1. The glass fraction in WTB waste can react in alkaline cementitious systems, while the epoxy resin may hinder glass dissolution. Because different WTB fiber sizes provide different extents of exposed glass surface, their reactivity in alkaline environments is expected to differ. To examine this hypothesis, alkali dissolution and reactivity tests were conducted on the WTB waste.

Hypothesis 2. Differences in the dissolution behavior of WTB waste may affect the hydration process of cement differently depending on fiber size. To address this hypothesis, isothermal calorimetry was performed on cement pastes containing different sizes of WTB waste, and the formed gels were further characterized by scanning electron microscopy (SEM).

Hypothesis 3. At the same fiber content in the cement matrix, smaller fibers with higher specific surface area may promote greater expansion, whereas longer fibers with lower specific surface area and a greater crack-bridging capacity may help restrain expansion.

These three hypotheses define the research framework of the present study and address key knowledge gaps related to the influence of WTB waste fiber size on hydration, microstructure, and ASR behavior in cementitious materials. Based on this framework, hydration products were characterized by powder X-ray diffraction (XRD), while X-ray computed tomography (XCT) and SEM were used to assess mortar microstructure. In addition, flexural strength, compressive strength, and ASR expansion were evaluated.

2. Materials and Methods

2.1. Materials and sample preparations

CEM I 52.5 R (Aalborg White, Denmark) was used as a Portland cement. WTB waste was sourced from Spain (PreZero). Before use in this study, the blade waste underwent a mechanical size-reduction process. According to the supplier preparation protocol, the blades were first cut into pieces, and metallic elements were removed. The material was then subjected to primary shredding using a twin-shaft pre-shredder, followed by secondary shredding using a crossflow shredder (chain mill) equipped with different screen sizes of 5, 15, 30, and 60 mm. This processing route generated heterogeneous fiber-like composite fragments containing glass fibers and epoxy resin. The overall processing route of the WTBW, from blade sections to shredded, sieved, and ground materials, together with the corresponding experimental workflow, is illustrated schematically in Fig. 1. The chemical composition of WTB waste and cement is listed in Table 1. The loss on ignition (950℃) of WTB waste and cement is listed as well. Then the content of the resin part is around 55 wt%, and the density of the WTB waste is around 1.66 g/cm^3. XRD diffractograms of cement and WTB waste are shown in Fig. 2, where the WTB waste shows a small amount of calcite, which is the filler material during the blade production [30,31]. The hump of WTB waste is the amorphous silicon compound.

Fig. 3 shows the WTB waste fiber passing by the sieves 63μm, 500 μm, 2 mm, and 8 mm with four different groups (63–500 μm, 500 μm~2 mm, 2–8 mm, and >8 mm). The fiber size in the study refers to the sieving size of the WTB waste fiber. The secondary electron scanning electron microscopy (SE-SEM) micrographs of each fiber group are also shown in Fig. 3 under each photograph of the fibers. SEM micrographs of the smaller WTB waste fibers show not attached epoxy resin particles around the glass fibers, while the large WTB waste fibers show more epoxy resin sticking to the fiber surface.

The mix design of the control samples and WTB waste-reinforced samples are listed in Table 2. The mortar mix design follows ASTM C1260 [32] and utilizes a concentration of 0.5 vol% of cement as fibers. Specially, standard steel fiber (6 cm × Φ1 mm) was also used as a control sample with fiber. The steel fibers were made of cold-drawn carbon-stell wire with a characteristic tensile strength of 1800 MPa, hooked ends (type 1 according to EN 14889–1: 2006 [33]). For this reason, the steel-fiber mixture (S8) shows a higher fiber mass than the WTB-based mixtures. This difference is expected and reflects the much higher density of steel fiber (7.85 g/cm^3) compared with WTB waste (approximately 1.66 g/cm^3). Deionized water was used as the mixing water for all paste and mortar mixtures. The same water source was used throughout all experiments. The sand used in the mortar was a 0/4 mm concrete sea sand (Class E) supplied by NCC Industry A/S, Denmark. According to the supplier declaration, the sand had a density of approximately 2.60 g/cm^3 and a water absorption of about 0.2%. The "W" represents the samples with WTB waste fiber, and the number afterwards represents the sieved size. The "S" represents the sample with steel fiber. The paste samples mix design for XRD and Isothermal calorimeter was the same as mortar samples without sand.

Mixture S8, containing steel fibers, was designed as a reference

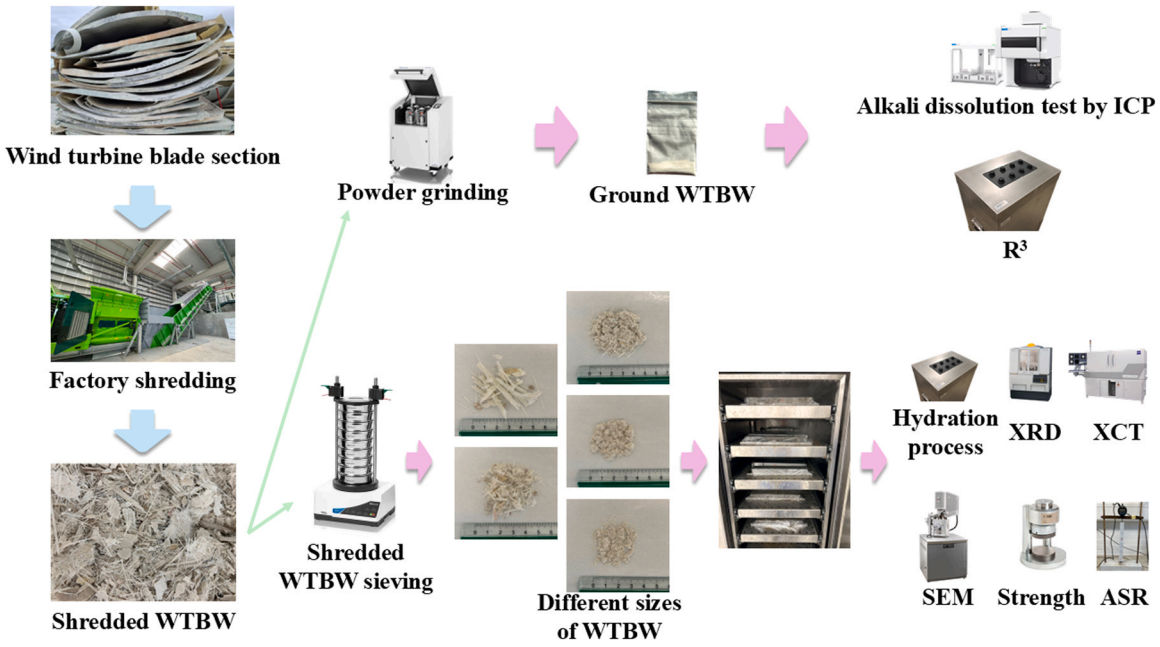

Fig. 1. Processing route and experimental use of WTBW in this study, showing blade sections, factory shredding, shredded WTBW, sieving into different size fractions, powder grinding, and the corresponding experimental methods applied to each material form.

Table 1
Materials compositions (wt%).

Group	Na_2O	MgO	Al_2O_3	SiO_2	SO_3	K_2O	CaO	TiO_2	Fe_2O_3	Others	LOI*
WTB waste	0.86	0.74	5.46	24.85	/	0.25	11.02	0.31	0.18	0.37	55.97
Cement	0.29	0.93	5.27	19.32	3.56	0.33	64.16	/	3.25	0.44	2.45

LOI*=Loss on ignition at 950℃

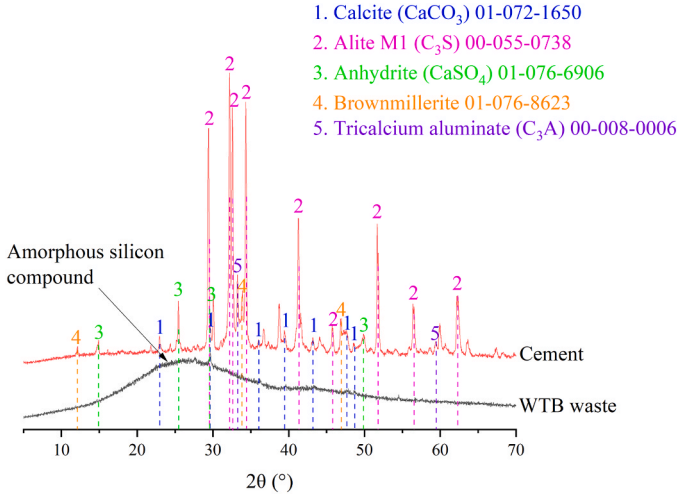

Fig. 2. XRD diffractograms of WTB waste (black) and unhydrated cement (red line).

mixture for selected tests rather than as a fully parallel comparator across all experimental evaluations. Because steel fibers differ fundamentally from WTB waste fibers in density, stiffness, morphology, and reinforcing mechanism, and because their strength contribution is substantially higher, S8 was used only where such a comparison was considered meaningful, particularly in the ASR assessment. The mortar composition adopted in this study was selected to provide a controlled cementitious matrix consistent with the ASR-related test program and suitable for isolating the effect of WTB waste fiber size. Therefore, the mixture design was not intended to represent an optimized sustainable mortar mix design or a direct equivalent of ordinary structural concrete, but rather a standardized matrix for investigating the feasibility of incorporating WTB waste as a fiber-type addition and for evaluating its influence on hydration, microstructure, mechanical behavior, and ASR expansion.

2.2. Testing methods

Alkali dissolution test

The WTB waste was ground down, and the mean diameter particle size was d_{50} = 23 μm. The alkali dissolution test was performed as described in [34]. Leaching of powdered WTB waste was carried out by mixing the powder with NaOH solutions with concentrations of 0.01, 0.1, and 1 M, in a solid to liquid (S/L) ratio of 0.05 g/ml up to 28 days. The dissolution process was carried out in a 500 ml plastic bottle and the slurry was placed on a shaking table with a constant speed of 200 rpm at room temperature (20℃). The leaching slurry was extracted and acidified at regular intervals after 10 mins, 1 h, 6 h, 1 day, 3 days, 7 days, 10 days, 14 days, 21 days, and 28 days then filtered. pH of the leachates were measured by senSION MM 374, the pH meter was calibrated by standard buffer solutions at pH of 10 before measurement. Then the leachates were analyzed for Ca, Si, Al, and Mg concentration by inductively coupled plasma emission spectroscopy (Agilent 5800 ICP-OES) with SPS 4 Autosampler.

2.2.1. Isothermal calorimeter

2.2.1.1. Hydration process. According to the mixture proportion in

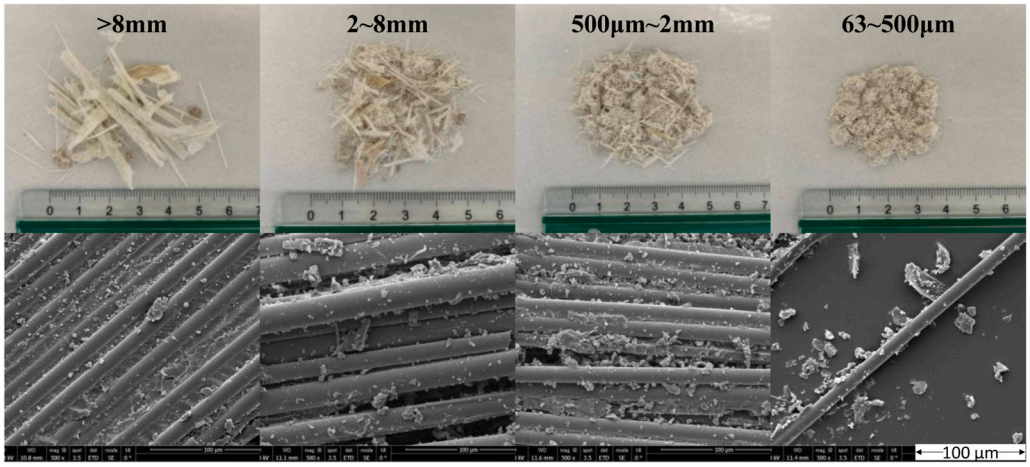

Fig. 3. Sieved fibers with different sizes photogram and SE-SEM micrographs.

Table 2
Mortar samples.

Sample ID	PC (g)	Sand (g)	WTB fiber (g)				Steel fiber (g)	Water/Cement	Note
			> 8 mm	2–8 mm	500um-2mm	63um-500um			
Ref	440	990	/	/	/	/	/	0.47	Control sample
W8	440	990	9.05	/	/	/	/	0.47	
W2	440	990	/	9.05	/	/	/	0.47	
W0.5	440	990	/	/	9.05	/	/	0.47	
W0.063	440	990	/	/	/	9.05	/	0.47	
S8	440	990	/	/	/	/	42.94	0.47	Control sample with steel fiber

Table 2, the heat evolution of the pastes (without the sand fraction) was measured with an isothermal calorimeter (I-Cal Flex, Calmetrix). In total 4.64 g of cement paste was used for each test group. Cumulative heat release and hydration exothermal rate are obtained and analyzed to study the hydration of WTB waste fiber reinforced cement matrix.

2.2.1.2. Rapid, Relevant and Reliable (R^3) test. The Rapid, Relevant and Reliable (R^3) test is used to assess the reactivity of powdered WTB waste (D_{50} = 23μm). The R^3 test was followed by ASTM C1897-20 [35]. Here, the cumulative heat of the reaction was measured in an isothermal calorimeter. All the pastes are injected into the sample container after a 2-minute mixing period. Heat flow and hydration heat data are continuously recorded for 7 days (168 h) at 20 °C instead of 40° C. All the paste ingredients, including the mixing solutions, were stored overnight at the same temperature as the test. The mix design of R^3 test can be found in Table 3. The compositions of the potassium solution are listed in Table 4.

2.2.2. Powder X-ray diffraction

Powder X-ray diffraction (XRD) analysis of WTB waste powder and WTB waste containing paste samples was conducted using a X Pert PRO instrument, which emitted Co-Kα radiation (40 kV, 30 mA). The scanning range for 2θ was set between 10 and 70°. The paste samples were crushed into powders and immersed in a 2-propanol solution for 24 h. Then the paste samples were dried under 40 °C for 24 h for the hydration stoppage process. All the samples (including raw WTB waste powder) were subjected to measurements with a step size of 0.05° and a counting time of 1 s per step.

Table 3
Mix design of R^3 test (unit:g).

	WTB waste	Sand	$Ca(OH)_2$	$CaCO_3$	Potassium solution
WTB	1		3	0.5	5.4
Ref-sand		1	3	0.5	5.4

Table 4
Potassium solution (unit:g).

	Potassium hydroxide	Potassium sulfate	Water
Mass	0.4	2	100

2.2.3. Micro-computed tomography (XCT)

A ZEISS Xradia 520 Versa scanner was employed to perform μXCT on −28 days old mortar cubic specimens (25 × 25 × 25 mm^3), incorporating 0.5% vol. of cement by WTB waste of the various sizes. Five specimens were investigated in total, each one representative of the groups illustrated in Table 2. Beam energy was set at 140 kV (10 W). A high-energy filter was used to optimize the X-ray beam transmission. The pixel size was equal to 35.2 μm, since the scan field-of-view (FOV) contained the entire specimen volume. The exposure time was 1.3 s. Binning was set to 1.0. A total of 1601 projections were acquired. A filter back-projection algorithm was applied for image reconstruction. The acquired 16-bit image data were converted to 8-bit, reducing the computational processing time. Avizo (ThermoFisher Scientific) was employed for 3D volume rendering applications, data visualization, and phase segmentation. Pore size distribution at the various systems, containing different WTB waste sizes was particularly studied.

2.2.4. Mechanical properties

Following a 28-day curing period at 20 °C and 95% relative humidity, flexural strength testing was conducted on the mortar bars (40 × 40 × 160 mm^3) by EN 196–1 [36]. The recorded strength value for each mix was determined based on the average of three samples. The testing involved applying a constant loading rate of 50 N/s until the fracture load was reached. The compressive strength testing was conducted on the remaining parts after the flexural strength test. The testing involved

applying a constant loading rate of 2400 N/s until the fracture load was reached.

2.2.5. Scanning electron microscopy

Post 28-day strength test, the remaining complete mortar parts were drilled to Ø 1 cm × 0.5 cm cylinders, which were impregnated with low-viscosity epoxy resin and then polished. The microstructure of the polished samples was coated by gold with 20 nm thickness and was examined by Quanta FEI FEG – 250 scanning electron microscopy (SEM) instrument with a Back-scattered Electron Detector (BSE). The composition of the gels (around WTB waste fiber in the matrix) was determined by energy dispersive spectroscopy (EDS) based on the SE graphs. The clusters of Ca-Si-Al were normalized by OriginPro 2024 to obtain data for ternary phase diagrams (Ca-Si-Al).

2.2.6. ASR test

The ASTM C1260 was utilized to conduct ASR testing of mortars containing WTB waste. The ABMT is widely employed for evaluating ASR potential reactivity in laboratory conditions due to its rapid response within 16 days. Mortar specimens with 25 × 25 × 285 mm^3 dimensions are produced and de-moulded after 24 h at 20 °C and 95% RH. Afterwards, they are subjected to a 24-hour curing period in water at 80 °C and subsequently, the specimens are immersed in a 1 M NaOH solution at 80 °C for 14 days. Moreover, extended exposure of the mortar bars in the alkaline solution (i.e., up to 28 days) can be used to achieve a more reliable assessment of the materials used.

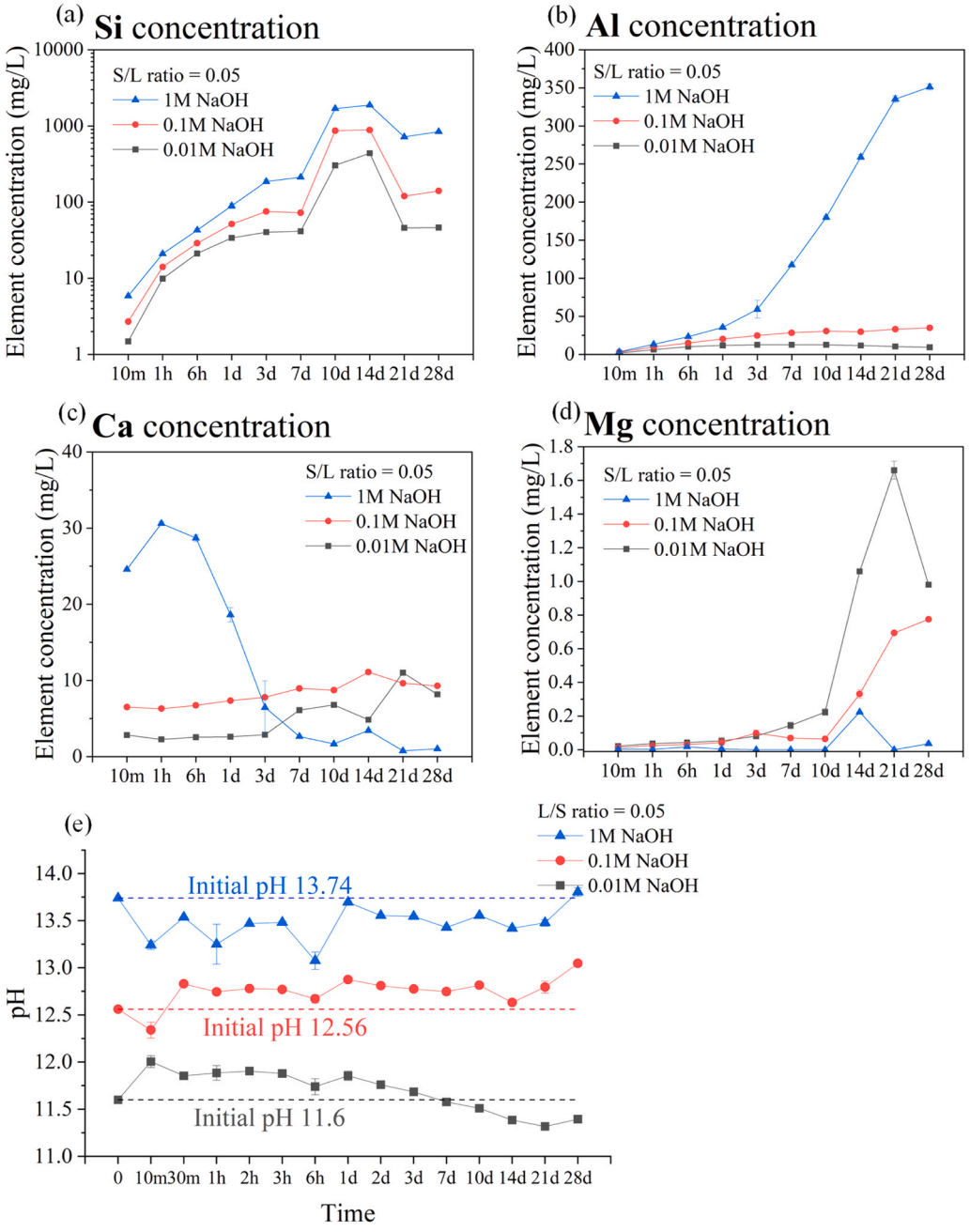

Fig. 4. Alkali dissolution testing with 0.05 S/L ratio (a) Si; (b) Al; (c) Ca; (d) Mg; (e) pH record.

3. Results and discussion

3.1. Characterization of raw WTB materials

3.1.1. Alkali dissolution test

The dissolution of ground WTB waste powder (D_{50} = 23 μm) in sodium hydroxide (NaOH) solutions at different concentrations with fixed solid-to-liquid (S/L) ratio of 0.05 was studied, and the results are shown in Fig. 4. These figures represent the release of silicon (Si), aluminum (Al), calcium (Ca), and magnesium (Mg) up to 28 days. The increasing concentration of NaOH leads to a faster breaking of Si-O and Al-O bonds, and hence highest Al and Si concentrations for 1 M NaOH solution, which is associated with the dissolution of Si and Al from glass fiber in WTB waste [37]. The pH variation during the tests was also measured to better understand the dissolution process.

Silicon (Si) Dissolution

The release of Si increased with higher NaOH concentrations, showing an initial rise and stabilizing after 7–10 days (in Fig. 4(a)). At 1 M NaOH, the Si concentration reached approximately 2000 mg/L by day 10, while lower concentrations of NaOH (0.1 M and 0.01 M) showed slower and lower dissolution rates. The higher NaOH concentration promotes the breaking of Si–O bonds in the glass fibers of WTB waste, releasing Si into the solution as $Si(OH)_4$. This dissolved $Si(OH)_4$ may later contribute to hydration reactions in cement-based materials.

Aluminum (Al) Dissolution

The release of Al followed a similar pattern to Si, but with a delayed start (Fig. 4(b)). The Al concentration in 1 M NaOH increased continuously, reaching around 250 mg/L after 28 days. The pH of the initial solution significantly influences the Al dissolution. The 0.1 M and 0.01 M NaOH show very low concentrations of Al dissolution. The Al dissolution from WTB waste may need minimum pH around 13.5.

The release of Al is attributed to the breakdown of Al–O bonds in the WTB waste. Once released, Al forms $Al(OH)_4^-$ ions in the alkaline solution. Together with Si, these dissolved species are key components for forming aluminosilicate gels during hydration reactions in alkali-activated or cementitious systems.

Calcium (Ca) Dissolution

Unlike Si and Al, the dissolution of Ca peaked early in the process and then decreased over time (Fig. 4(c)). Ca reached its maximum concentration (~30 mg/L) within 1 h in 1 M NaOH and then gradually decreased as the test progressed. Coinciding with Ca precipitation in the form of calcium hydroxide ($Ca(OH)_2$) and possibly aluminosilicate gels. These reactions remove Ca^{2+} from the solution, contributing to the observed decrease in Ca concentration. The dissolved Ca, along with Si and Al, may also participate in forming hydration products like C(N)-A-S-H gels, which are responsible for binding and strength development in the cementitious binders.

Magnesium (Mg) Dissolution

The behavior of Mg was different from Si, Al, and Ca (Fig. 4(d)). Mg showed the highest concentrations at lower NaOH concentrations (0.01 M and 0.1 M), while very little Mg was released in 1 M NaOH. The limited release of Mg in highly alkaline conditions is due to its low solubility at elevated pH, as the precipitation of $Mg(OH)_2$ is favored ($K_{sp} = 1.5 \times 10^{-11}$). Additionally, the small amount of Mg in the WTB waste limits its overall release into the solution.

pH Variation

The initial pH of the solutions, determined by the NaOH concentration, was 13.74 for 1 M NaOH, 12.56 for 0.1 M NaOH, and 11.6 for 0.01 M NaOH (Fig. 4(e)). The pH varies at 10 min, 6 h, and 10d for 1 M NaOH. For 0.1 M and 0.01 M NaOH, a gradual decrease in pH was observed over time. This drop is attributed to the consumption of OH^- ions during the dissolution of WTB waste and the precipitation of reaction products like $Ca(OH)_2$ and aluminosilicate gels.

It needs to be noted that Ca concentration at 0.05 S/L (shown in Fig. 4) starts to decrease after 1 h of the alkali dissolution process. Firstly, the decrease in Ca concentration is related to forming portlandite ($Ca(OH)_2$) and possible aluminosilicate gels as mentioned. Sufficient Ca^{2+} and OH^- lead to the precipitation of the $Ca(OH)_2$, simultaneously, Ca^{2+}, $Si(OH)_4$, and $Al(OH)_4^-$ lead to the precipitation of the amorphous gels [38]. Mg shows an adverse trend of dissolution compared to Si, Al, and Ca elements. The higher pH of the dissolving solution leads to a lower release of Mg^{2+} into the aqueous environment [39]. Simultaneously, only limited Mg^{2+} ions are identified in the dissolving solution because of the limited Mg source from WTB waste. The results indicate that higher NaOH concentrations accelerate the dissolution of Si, Al, and Ca from WTB waste, providing essential components for hydration reactions in cementitious systems. The findings highlight the dissolution mechanism of how the alkalinity of the pore solution influences WTB waste in cementitious composites.

3.1.2. Rapid, Relevant and Reliable (R^3) test

Fig. 5 shows the normalized cumulative heat release of WTB waste fibers (mixed with the potassium solution, portlandite, and calcite powder) and sand reference sample (mixed with the potassium solution, portlandite, and calcite powder) are measured by an isothermal calorimeter (R^3 test) for 14 days at 20°C. Fig. 5, shows the heat release curve. After 40 h, the heat release curve increases, and this is due to the pozzolanic reactivity of WTB. The glass fiber content in WTB starts to contribute to the hydration process under normal temperatures (20°C) [40]. As mentioned in the alkali dissolution test, WTB waste dissolves sufficient Ca^{2+}, $Si(OH)_4$, and $Al(OH)_4^-$, leading to the precipitation of the amorphous gels. This proves the pozzolanic reactivity of WTB in the cement/concrete matrix as a potential supplementary cementitious material. The Ref-sand shows very limited heat release of mixing solutions (from the portlandite).

3.2. Characterization of WTB waste-containing composites

3.2.1. Isothermal calorimetry

Fig. 6 shows the normalized heat flow and total heat release of WTB waste in the cement matrix. Fig. 7 shows the time to reaction peak (TTRP) and height of the peak (HOP) based on the calorimetric results in Fig. 6. TTRP refers to the time from the beginning of the test to the second exothermic peak (related to the formation of reaction products), and HOP is the heat flow of the second exothermic peak [41].

As can be seen in Fig. 6, W0.063 shows the lowest normalized heat flow in the acceleration/deceleration period. At the same time, W0.063 also has the highest total heat release after a 7-day calorimetric

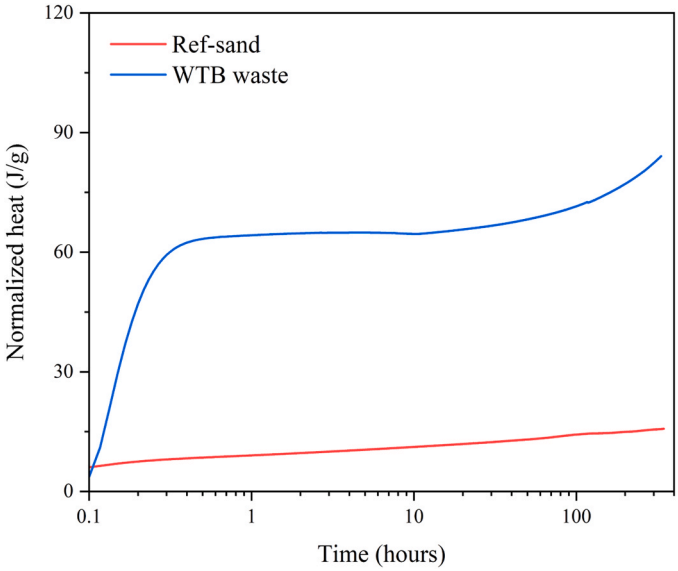

Fig. 5. Pozzolanic activity of WTB waste.

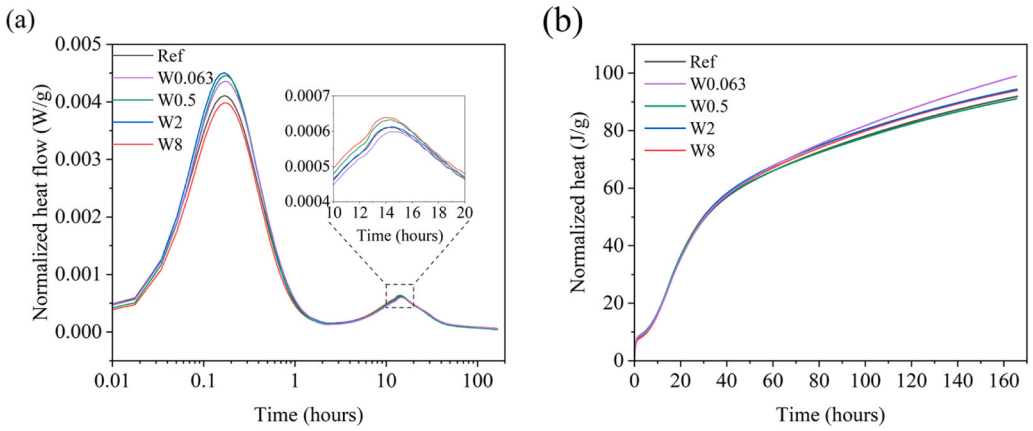

Fig. 6. WTB waste in cement (a) Normalized heat flow; (b)Normalized total heat release.

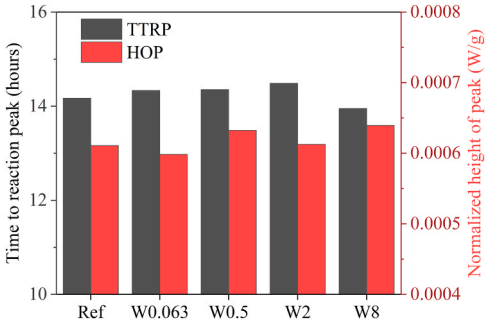

Fig. 7. Time to reaction peak and height of the peak of WTB waste in cement.

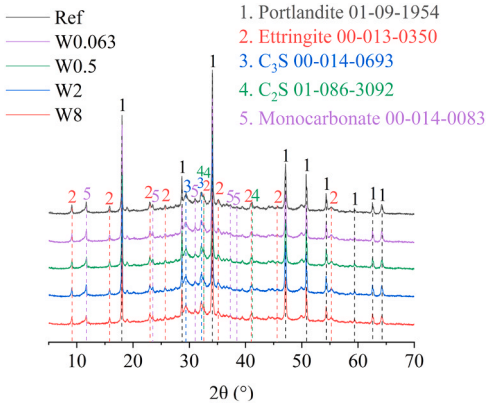

Fig. 8. XRD of WTB-containing cement pastes at 28 days.

experiment. This is due to the small particle size of the W0.063 fiber. The finer particle size of WTB waste leads to a more specific surface area of glass content in an alkaline environment in cement. The glass content may consume the alkalinity of the pore solution [42]. This leads to a low heat flow at the early hydration process but contributes to the total heat release after 7 days. This is in line with R^3 test results that WTB waste starts to generate heat after 7 days.

Generally, TTRP and HOP decrease with the fiber fractions from Fig. 7, and WTB-containing samples show longer TTRP than the control sample. Because the WTB waste may absorb extra water, leading to a delay in the hydration process [31]. However,W8 shows the fastest TTRP with the highest HOP. This is due to the sieving size of fibers (> 8 mm), which results in less water absorption and the pH value of the pore solution. In other words, less alkaline pore solution contact with WTB (>8 mm) leads to more available alkalis for cement hydration. This will accelerate the hydration process of the cement matrix. Also, the available alkalis may lead to higher ASR in the late hydration state. While WTB fibers in W2, W0.5, and W0.063 have higher specific surface area than W8, more alkalis are needed for the dissolution of glass content. Consequently, the delay hydration peaks are observed. The finer WTB particles will continue to the late hydration process as mentioned. The heat release is more obvious up to 7 days.

3.2.2. *X-ray diffraction (XRD)*

Fig. 8 shows the XRD patterns of the 28-day pastes. There is a small difference between the control samples and the WTB waste-containing. All peaks generally occur at the same positions irrespective of different samples. This means fiber fractions will not impact the types of cement hydration products during the first month of hydration. The typical portlandite peak dominates in all paste samples. The extra $Ca(OH)_2$ may provide enough alkalinity for the further reaction of glass content in the WTB waste fiber. This may be reflected in the strength in a very late curing age. Simultaneously, the remaining C_3S and C_2S will continue to the late hydration process under an ambient environment. Besides, no distinct peak of calcite from the embedded WTB waste fibers is identified. This is due to the small percentage of the encapsulated WTB waste fibers compared to cementitious materials.

3.2.3. *Micro-computed tomography (XCT)*

Representative 2D orthoslices originating from the reconstructed XCT data are illustrated in Fig. 9(a) for all specimens imaged. A detailed illustration of the phase segmentation process is also given (Fig. 9(b)). UC and CM&W stand for un-hydrated cement, cement matrix, and waste.

Three main phases were distinct, based on the grayscale intensity distribution, including the low-intensity region associated with the porosity and air voids, the medium-intensity region linked with the hydrated cement matrix, sand particles, and glassy fibrous content of the WTB waste, and the high-intensity region associated with the un-hydrated cement particles. The porosity/voids spatial distribution within the five specimens is illustrated in Fig. 10.

Porosity variations can be observed between the five systems. Large distinct pores are detected in systems W0.5, W2, and W8, while the reference and W0.063 specimens display a more uniform size distribution. A detailed quantitative analysis was performed to determine the pore size distribution. The results are presented in Fig. 11. Both the total number of pores (Fig. 11a), cumulative pore volume (Fig. 11b), and pore frequency histogram (Fig. 11c) are given. A relative correlation can be observed between the fiber size used in the batch and the total number of pores. The reference specimen contains the largest number of pores, with W0.063 following. A completely inverse trend is observed for the

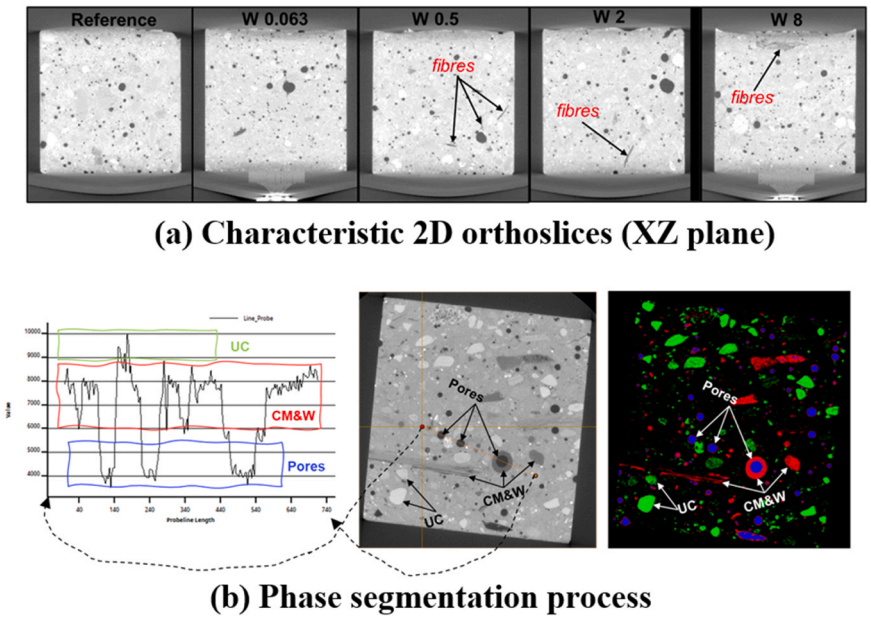

Fig. 9. Illustration of (a) characteristic 2D views of the tomograms acquired for the various specimens along with (b) phase segmentation protocol, including a characteristic line scan example (based on 16-bit data). UC and CM&W stand for un-hydrated cement, cement matrix, and waste.

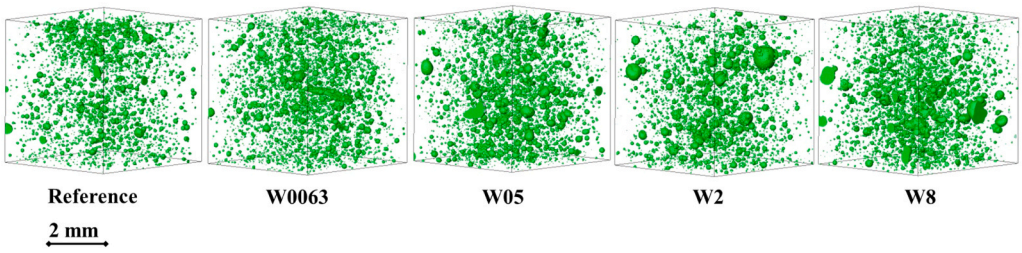

Fig. 10. Representative 3D views of porosity/air void spatial distribution for the five mortar specimens subjected to X-ray imaging.

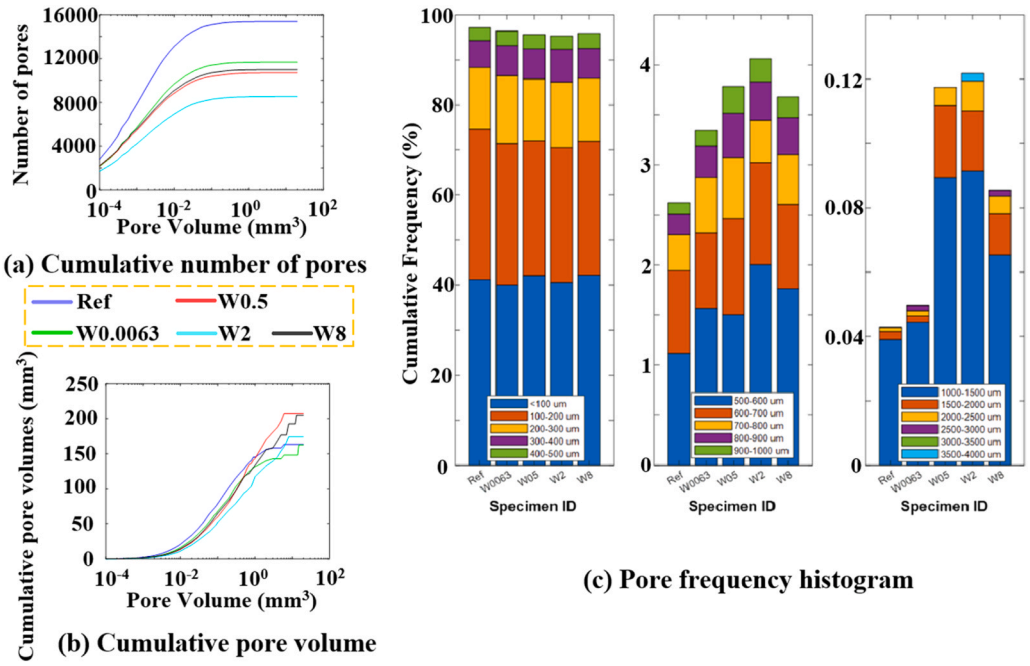

Fig. 11. Distribution of (a) Cumulative number of pores, (b) cumulative pore volume, and (c) pore frequency histogram among the five specimens.

cumulative pore volume. Fig. 11(b) shows the evolution of pore volume, which can be divided into three stages. The first stage (only pores lower than 0.5 mm^3 are considered) is characterized by a linear growth rate of the pore volume with the reference and W0.063 specimens being the most porous while the W2 exhibits the lowest pore volume. A second stage (0.5 mm^3 < pore volume < 2 mm^3) can be distinguished, where the first differences among the five systems are spotted. The linear growth rate of cumulative pore volume persists for the specimens containing larger-size fibrous elements, i.e., W0.5, W2, and W8, while a growth rate decay is observed for the reference and the W0.063 specimens. The last stage (2 mm^3 < pore volume < 5 mm^3), including the largest volumes, indicates an intensified behavioral shift among the five specimens. The reference and W0.063 specimens show no further growth of the cumulative pore volume within this range (further increase can be spotted when pores larger than 5 mm^3 are considered). On the contrary, a linear growth rate of the cumulative pore volume persists for W05, W2, and W8 specimens. Fig. 11(c) illustrates the differences in the pore frequency histogram among the five systems. Small-sized (equivalent diameter < 0.5 mm) pore distribution is relatively uniform among the specimens, with more than 40% of the pores having an equivalent diameter (ED) less than 0.1 mm. Medium-sized pores (ED is between 0.5 and 1.0 mm) lie within a range of 2.5% - 4% of the pore population, while the corresponding range for large-sized pores (ED > 1 mm) is 0.04% - 0.12%. To sum up, the cumulative pore volume is higher for the specimens containing larger-sized fibrous elements (W0.5, W2, and W8), even though these specimens contain fewer pores.

This behavior is attributed to the presence of isolated large pores (ED > 1.0 mm) in the specimens containing large-sized fibrous elements (W0.5, W2, W8), which is not observed for the specimens containing either small-sized fibrous elements (W0.063) or no WTB waste (reference). The mean pore volume index, defined as the ratio between the cumulative pore volume and total number of pores was employed to enhance comparison between the five different systems studied. The results are presented in Fig. 12 and the detailed porosity values are presented in Table 5. It is worth noting that the mean pore volume index grows with increasing size of the embedded fibrous elements until a peak is reached (W2 specimen), followed by a decay as the size of the embedded waste further rises (W8 specimen).

3.2.4. Scanning electron microscopy

Representative SEM micrographs of 28d mortar samples are shown in Fig. 13. W8 shows a large area of epoxy resin with a cluster of glass fibers. This is associated with the large size of WTB waste containing more epoxy resin coating than the smaller sizes. This has been proven by SEM of WTB waste in different sizes (Section 2.1, Fig. 3). The epoxy resin surrounds the inner part of the glass fiber preventing the attack from the alkali pore solution. Thus, glass fibers with perfect round shape can be observed both in W8 and W2. However, the glass fiber in W0.063 has no protection from the resins. The glass fiber exposes to the alkali pore solution directly, leading to a fast dissolution of glass fiber. Therefore, the glass fibers in WTB waste lose the round shapes. This can be due to polishing artifacts, but the broken glass fibers can be found not in one spot under the SEM graphs.

Table 5
Porosity by XCT (vol%).

	Ref	W0.0063	W0.5	W2	W8
Porosity	1.45	1.45	1.84	1.80	1.83

Fig. 14 shows EDS maps of mortar samples at 28 days. W8, W2, and W0.5 illustrate the typical shapes of glass fiber from WTB waste. The overlap of Ca, Al, and Si is the location where the fiber is. WTB waste fiber shows a higher Al content than the cement matrix. In addition, the sand can be easily distinguished by the overlap of Si and O. It is worth noting that the Ca content in WTB waste shows more brightness than in the gel matrix. At the meantime, Si content in WTB waste is more intense than in the gel matrix. Those are all in line with XRF results (Table 1).

To further understand how WTB waste influences the formation of C-S-H gels, Fig. 15 exhibits the EDS dots and a ternary graph of Ca, Si, and Al. Each sample has 25 EDS dots on the amorphous gels near the WTB waste fiber. As can be seen from the ternary graph, W8 shows large ranges of Ca distribution, which represents a low Ca content in the amorphous gels. This finding is associated with the epoxy resin confinement effect induced on the embedded glass fibers, as mainly observed in the systems containing large-size WTB waste. The epoxy resin acts as a protective barrier to the confined glass fiber, decelerating glass dissolution. On the contrary, W0.063 and W0.5 contain high Ca content in the gels. This is due to the fast dissolution of glass fiber in WTB waste. As proved in Section 3.1.1, Ca in WTB waste can be released to alkali solutions very fast. This phenomenon is highly related to the particle size of WTB waste. The smaller size of WTB waste results in the fast dissolution of glass, which leads to a high Ca release. Ca can be captured by silicate monomers, generated via dissolution of the cement particles, forming Ca-rich amorphous gels.

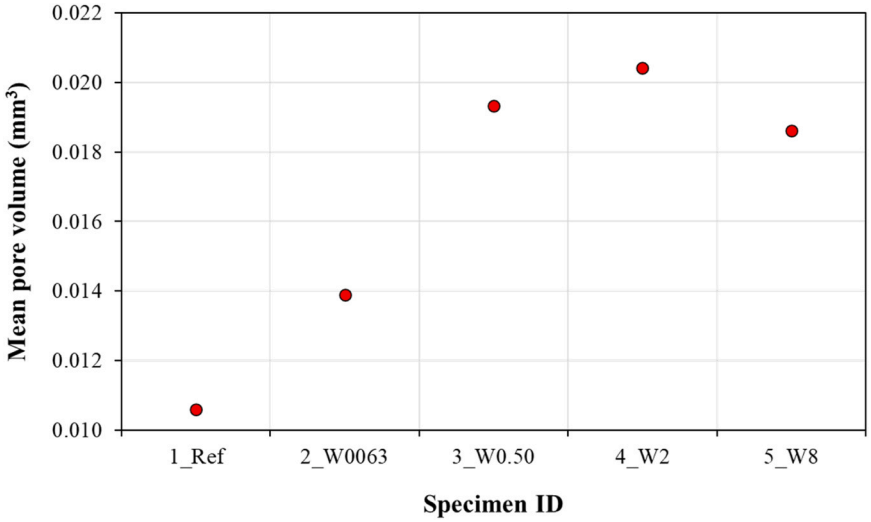

Fig. 12. Mean pore volume index variation for the five systems studied via X-ray imaging.

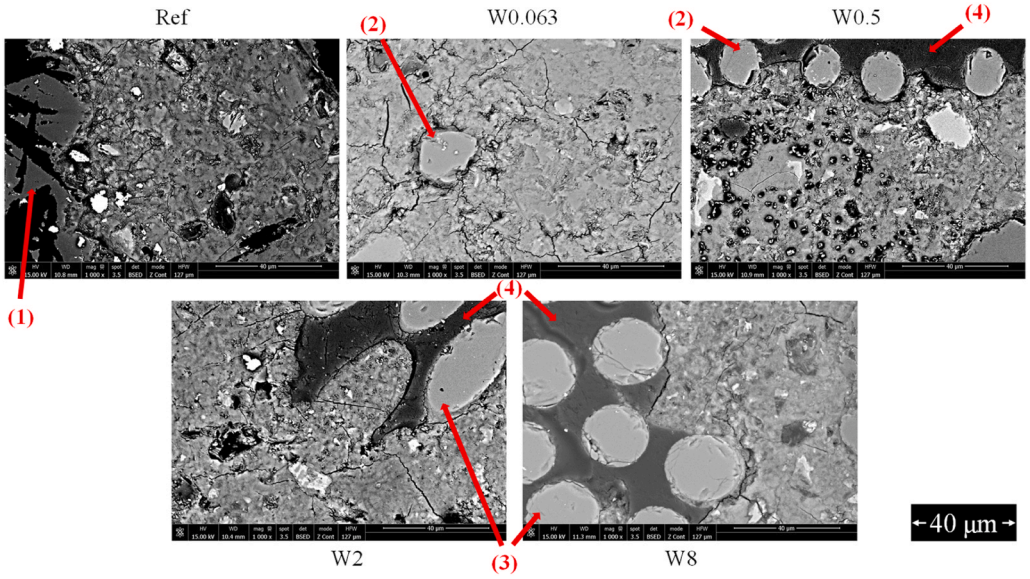

Fig. 13. SEM micrographs of each mortar sample at 28 days (1) Sand; (2) Broken glass fiber; (3) Completed glass fiber; (4) Epoxy resin.

3.3. Properties of WTB-waste containing composites

3.3.1. Strength

Fig. 16 (a) shows the flexural and compressive strength of WTB waste-containing mortars at 28 days. The flexural strength of Ref, W0.063, W0.5, W2, and W8 are shown in Table 6. W2 exhibits the highest flexural strength among the samples, exceeding the flexural strength of W8, which contains larger-size fibers. This paradox can be linked to the orientation of the embedded WTB fiber in the samples. Additionally, some fibers may be perpendicular to the tensile stress distribution, and no significant contribution is expected to resist the tensile forces [43]. This results in a limited improvement in flexural strength. However, they can help in controlling crack propagation in other directions. The compressive strength of Ref, W0.063, W0.5, W2, and W8 are shown in Table 6. Generally, the compressive strength is expected to increase with smaller sizes of WTB waste fibers. As mentioned in Section 3.2.4, the smaller size of WTB fibers tends to dissolve more Ca into the pore solution. However, other factors can also affect the material strength, including the fiber length and, as already mentioned, fibre orientation. Thus, it shouldn't be a paradox to note that W2 sample shows the highest compressive strength among the samples. Longer fibers can act as crack-bridging agent, and thus, contribute to a higher compressive strength, due to the increased toughness of the samples (as shown in Fig. 16 (b)).

3.3.2. ASR tests

Because WTB waste contains glass-rich phases, its incorporation into cementitious materials raises a potential alkali–silica reaction (ASR) risk under alkaline exposure. Therefore, beyond mechanical performance, the ASR test is essential for assessing the durability-related feasibility of using WTB waste in mortar. The results of ASR kinetics and expansion amplitude, according to the specifications outlined in ASTM C1260, for all the mixtures developed in the laboratory are highlighted in this section. The expansion kinetics and final expansion amplitudes were analyzed for mortar samples incorporating four different ranges of WTB's particle sizes; the control mixture (Ref); and a second reference incorporation steel fibre (SF). The measured expansions over a 28-day exposure period in a 1 M NaOH solution are presented in Fig. 17. [37–41]

At 14 days, mixtures containing the finest WTB particles (W0.063 and W0.5) exhibited the highest expansion values (both reaching 0.17%), demonstrating a rapid ASR reaction, likely due to their increased surface area and enhanced reactivity. The W2 mixture initially exhibited lower expansion than the control (N) until 9 days; however, an accelerated increase in expansion amplitude was observed thereafter, reaching 0.16% at 14 days, comparable to the most reactive mixtures. This suggests a delayed onset of ASR expansion, potentially due to the epoxy protection slowing the initial dissolution of silica from WTB waste but later contributing to substantial expansion.

The W8 mixture showed an expansion amplitude of 0.13% at 14 days, closely resembling the control sample (N = 0.14%). However, its expansion kinetics changed significantly between 14 and 28 days, exhibiting a steeper increase than all other mixtures, ultimately reaching 0.21%—one of the highest final expansion values recorded. This delayed but pronounced ASR reaction suggests that while larger WTB particles initially suppress ASR, their long-term behavior results in significant expansion, possibly due to a gradual breakdown of the protective epoxy matrix and increased exposure to the alkaline solution. At 28 days, W2 recorded the highest expansion (0.23%), indicating a steep increase beyond 14 days, further confirming its delayed yet aggressive ASR development. Similarly, W8, which initially followed the control's expansion trend, experienced an expansion acceleration, surpassing both the control and the finer WTB mixtures. Notably, the steel fibre-reinforced mixture (S8) exhibited the lowest expansion, stabilizing at 0.10% from 14 to 28 days. The better performance of the SF mixture is attributed to its mechanical restraint on expansion stresses.

4. Further discussions and perspectives

4.1. Dissolution of WTB waste under a cementitious environment

Fig. 18 illustrates the dissolution processes of wind turbine blade (WTB) waste when exposed to an alkaline solution (as a model for alkaline pore solutions of cementitious matrix). Fig. 18 demonstrates the transformation of materials as the pH level increases and includes a detailed representation of the WTB waste particle and the chemical species dissolved from it.

According to the alkali dissolution test (Section 3.1.1), the test was simulated under different pH levels to simulate behavior of WTB waste under different pore solutions of cementitious materials. As the alkaline solution begins to act on the WTB waste particle, ions such as Ca^{2+}, Mg^{2+}, $Si(OH)_4$, and $Al(OH)_4^-$ start to dissolve from the exposed glass fiber. At higher pH, more of the WTB material dissolves, releasing additional Ca^{2+}, Mg^{2+}, $Si(OH)_4$, and $Al(OH)_4^-$ ions into the alkaline

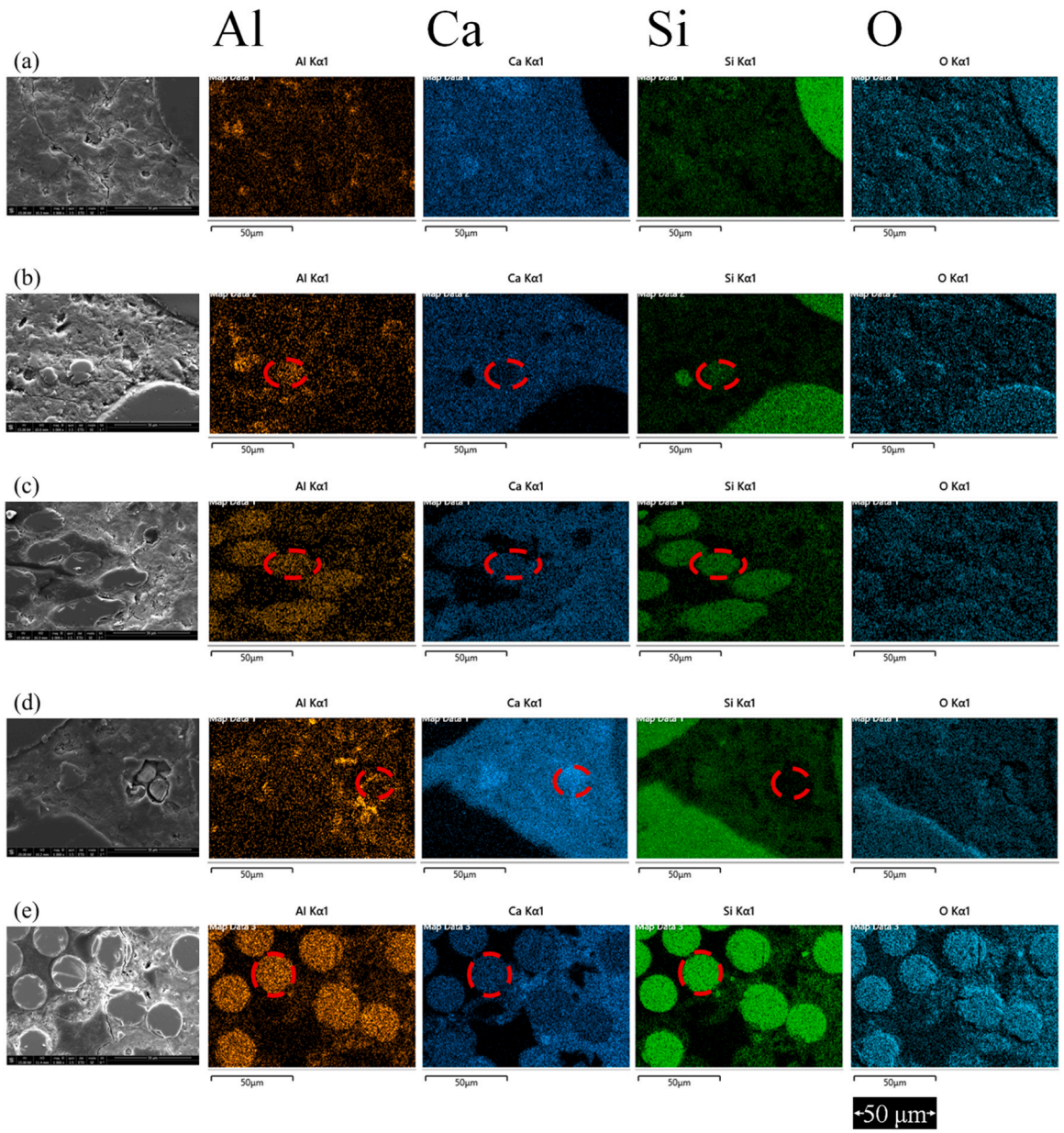

Fig. 14. EDS mapping graphs of mortar samples at 28 days (a) Ref; (b) W0.063; (c) W0.5; (d) W2; (e) W8. (Red dash circles are the positions of WTB waste fiber).

solution (comparable to the pore solution of the cementitious matrix). As dissolution progresses, this facilitates the formation of calcium-aluminum-silicate-hydrate C(N)-A-S-H gels, possibly the formation of $Ca(OH)_2$ (in GEMS simulations, ultimately it transfers to C(N)-A-S-H gels) (In Supplementary Materials). Simultaneously, more $Mg(OH)_2$ is also formed as the pH increases. The R^3 test also shows the reactivity of WTB waste materials under the environment of the pore solution in cementitious materials. This further proves that higher pH can lead to more dissolution of glass content in the WTB waste. The presence of OH^- ions in the solution promotes further breakdown of the glass fiber, leading to more extensive dissolution and release of calcium, silicate and aluminate ions. The pH increase promotes higher dissolution of WTB waste and more formation of C(N)-A-S-H gels and $Mg(OH)_2$, highlighting more dynamic interaction between WTB waste and the alkaline solution.

Fig. 19 illustrates the relationship between fiber size and the dissolution of glass content, specifically focusing on the release of Ca^{2+}, $Si(OH)_4$, and $Al(OH)_4^-$ ions from WTB waste in an alkaline solution. This indicates an inverse relationship between fiber size and the dissolution of glass content: smaller WTB waste fiber size has a more intensive shredding process, leading to greater exposure of glass fibers and more extensive interaction with the alkaline solution. This results in increased dissolution of Ca^{2+}, $Si(OH)_4$, and $Al(OH)_4^-$ ions from the glass fibers. It can be seen from the SEM graphs that the smaller WTB waste fiber almost loses the round shape under the alkali attack from the pore solution. In the contrary, larger WTB waste fiber size has more epoxy resin (shown in the SEM graph) encapsulating the glass fiber, reducing their exposure to the alkaline solution. Consequently, the dissolution of Ca^{2+}, $Si(OH)_4$, and $Al(OH)_4^-$ ions are lower.

Overall, the dissolution of Ca^{2+}, $Si(OH)_4$, and $Al(OH)_4^-$ ions from WTB waste are strongly dependent on the size of the WTB waste fibers. This relationship is critical for understanding the reactivity and material stability in the pore solution of cementitious materials. These findings prove Hypothesis 1 that WTB waste shows material properties as SCMs (fine particle) under an alkaline environment.

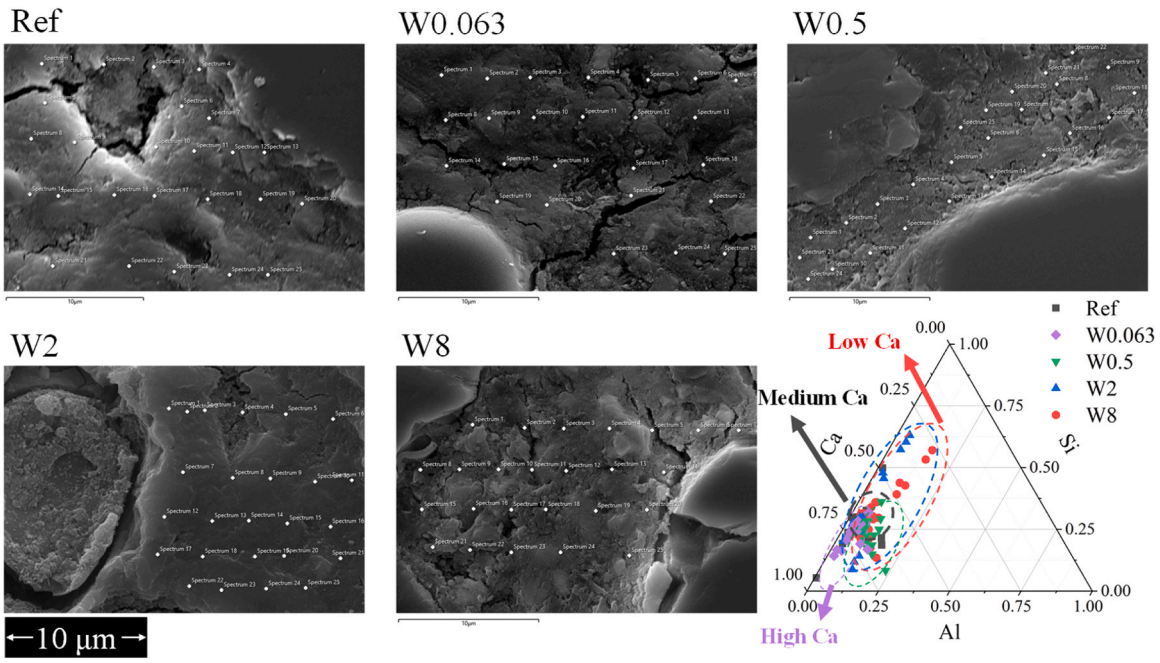

Fig. 15. EDS dots and ternary graph of Ca, Si, and Al.

(a)

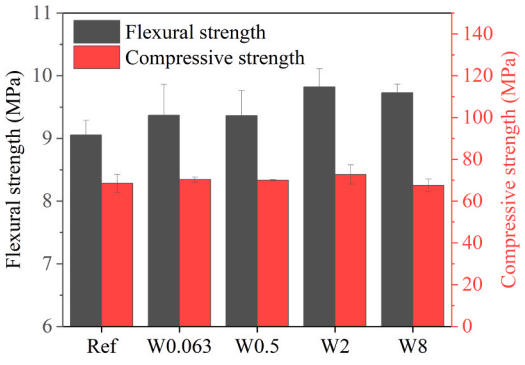

(b)

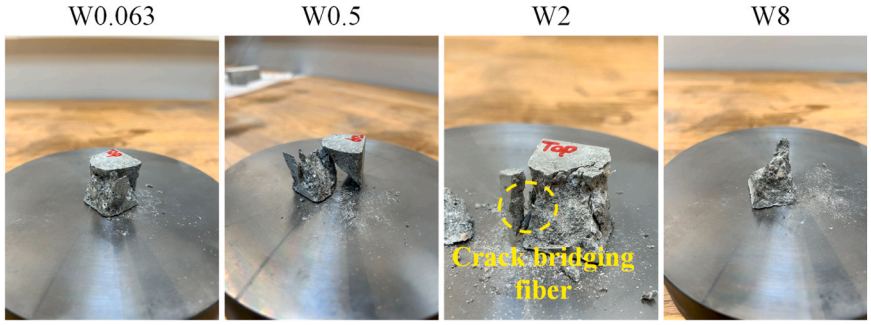

Fig. 16. (a) Flexural and compressive strength of mortars at 28 days; (b) Broken cubic mortars after compressive strength test at 28 days.

4.2. *Effect of WTB waste size on cement hydration*

Fig. 20 shows the effect of WTB waste fiber size on the cement hydration process, with correlations on the calcium (Ca) atomic ratio in the formed gels (from SEM EDS) and calorimetric heat release.

As fiber size increases, there is a notable change in both the Ca

Table 6
Strength results at 28 days (MPa).

	Ref	Std*	W0.063	Std*	W0.5	Std*	W2	Std*	W8	Std*
Flexural strength	9.06	0.23	9.37	0.69	9.36	0.40	9.82	0.29	9.73	0.14
Compressive Strength	68.47	4.32	70.30	1.27	67.02	0.29	72.72	4.59	67.53	3.04

Std* = Standard deviation

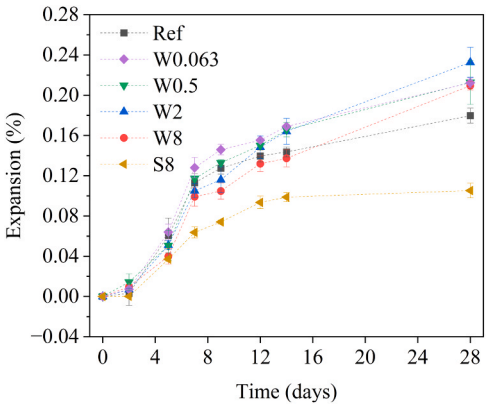

Fig. 17. ASR of WTB-waste containing mortar.

atomic ratio range and the height of the hydration peak. Small WTB waste fiber size has a high Ca atomic ratio range in formed gels. This is due to smaller particles having a higher surface area and more exposed glass fiber, leading to the more extensive dissolution of calcium ions as explained in Section 4.1. The higher dissolution rate of calcium ions consumes more OH^- ions at the early hydration process, simultaneously, the more exposed epoxy resin particle also consumes OH^- ions due to the ring-opening reaction, both resulting in a decrease in heat release. This slightly delays the hydration reaction causing a lower height of peak. The small WTB waste fiber size shows a powder-like rather than a fiber-like behavior in the cement matrix. On the contrary, large WTB waste fiber size leads to less dissolution of calcium ions due to the epoxy wrapping around the glass fiber. The reduced dissolution rate of calcium ions leads to less consumption of OH^- ions at the early hydration process. A resulting higher hydration reaction leads to a higher height of peak. As can be seen from Fig. 7, there is a tiny increase from W0063 to W2 in TTRP, but a decrease in W8. These findings reveal Hypothesis 2 that the encapsulation of large-size fiber fraction accelerates the cement hydration process, compared to smaller-size waste.

4.3. Effect of WTB waste size on matrix performance

Fig. 21 illustrates the impact of fiber size on porosity, further to ASR expansion and compressive strength in a cement matrix. The figure includes data for different fiber sizes (0.063–0.5 mm, 0.5–2 mm, 2–8 mm, and >8 mm), showing matrix porosity, expansion, and compressive strength.

Porosity in the cement matrix affects its mechanical properties, with lower porosity typically leading to higher strength. Lower porosity values are observed with the incorporation of small WTB waste fiber sizes (0.063–2 mm). The bridging effect of small fibrous elements seems to be more vital than porosity and pozzolanic activity. The small WTB waste fiber sizes (0.063–2 mm) show typical powder behavior. The pozzolanic activity of WTB waste leads to more dissolution of glass fiber and the formation of gels. Pozzolanic reactions occur when siliceous materials (e.g., glass fibers) react with calcium hydroxide in the presence of water to form amorphous gels, which contribute to the strength of the cement matrix. The formed gels lead to a higher ASR expansion with smaller WTB waste fiber sizes.

Medium WTB waste fiber sizes (2–8 mm) demonstrate a special powder-fiber behavior. On the one hand, the small-size particles in this range show the pozzolanic activity of glass content leading to more formation gels, and higher expansion of the matrix. On the other hand, the large-size particles in this range show the fiber behavior retaining the expansion of the matrix.

A high porosity value is observed with larger WTB waste fiber sizes (>8 mm). The incorporation of larger-size WTB waste fiber introduces more defects into the cement matrix. While the large-size WTB waste fiber has more epoxy resin around the glass fiber. This protects the glass from the attack of the alkaline environment, leading to better durability of the fiber. The larger WTB waste fibers (>8 mm, typically fiber behavior) retain more expansion of the matrix, indicating higher effective mitigation of ASR.

From an engineering perspective, these results show that the suitability of WTB waste in mortar cannot be evaluated only by strength development, but must also consider the durability risk associated with ASR, which is strongly influenced by fiber size and the extent of exposed

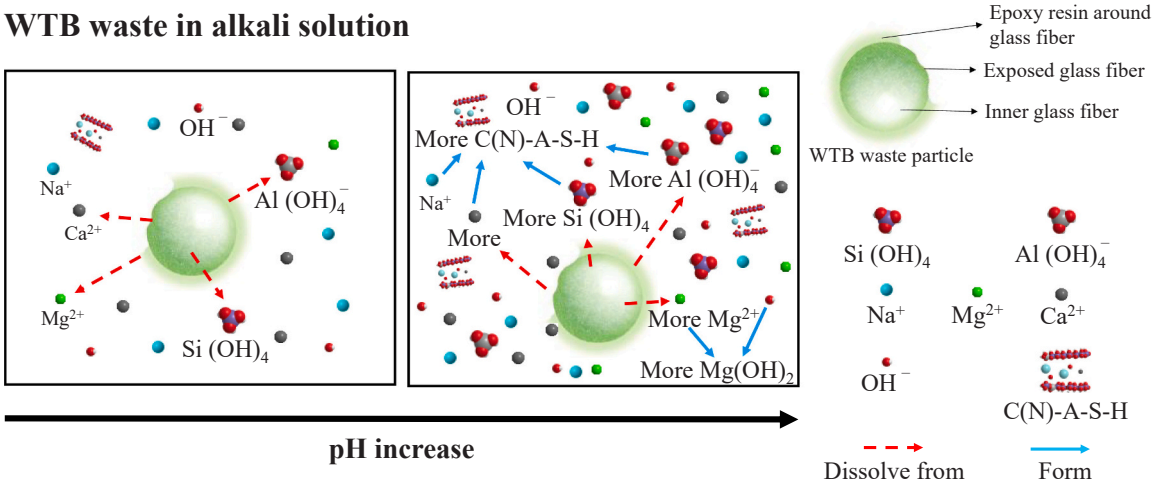

Fig. 18. Effect of pH on the dissolution of WTB waste and precipitation.

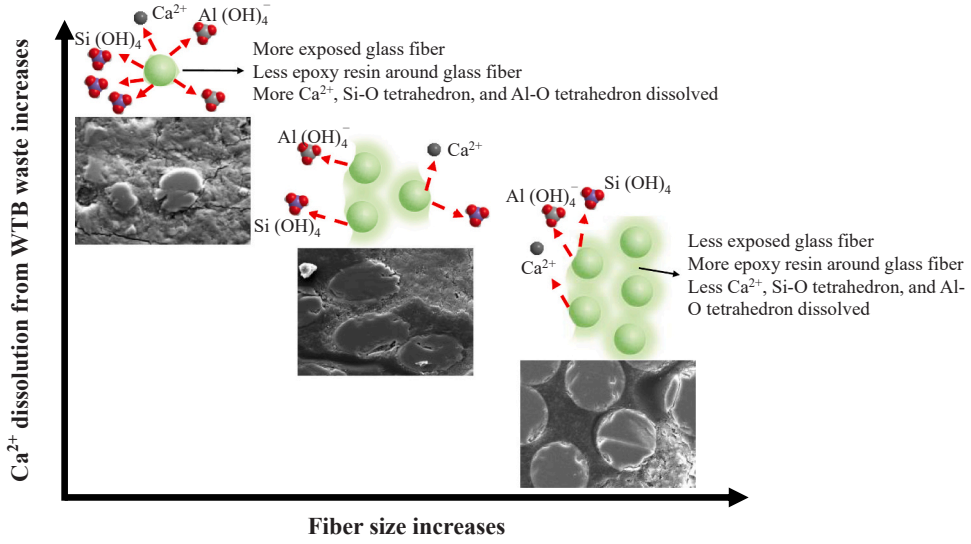

Fig. 19. Effect of fiber size on the dissolution of WTB waste.

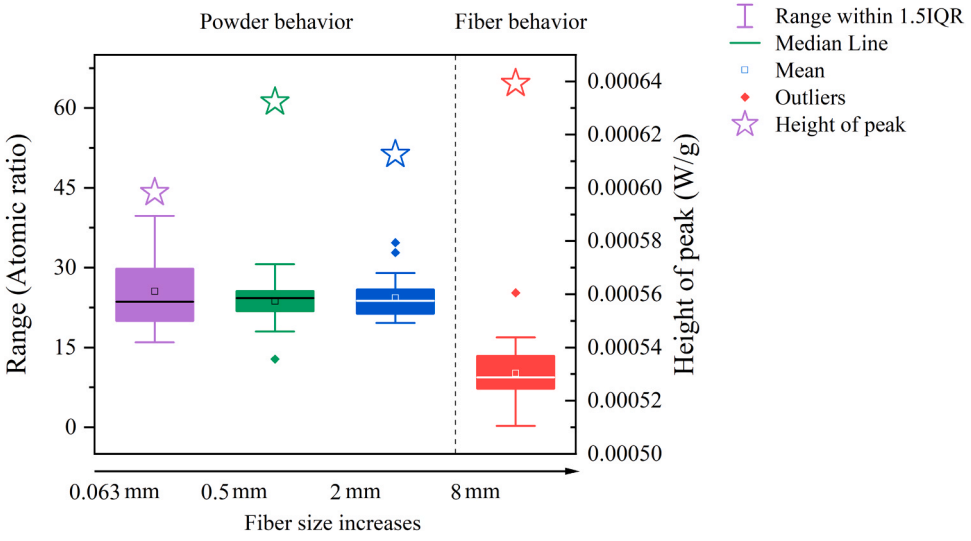

Fig. 20. Effect of WTB waste fiber size on cement hydration.

glass. This durability-oriented perspective is consistent with recent studies showing that WTB-derived recycled fractions can increase porosity and modify water-transport behavior in cementitious materials, even when their mechanical use remains feasible [44]. Overall description answers Hypothesis 3 that small WTB waste fibers (0.063–2 mm) demonstrate pozzolanic activity due to the exposed glass fibers, while larger WTB waste fibers (>8 mm) have glass fibers covered in epoxy resin, which contributes to improved durability of the matrix. Although the present study focuses on separated WTB size fractions in order to clarify size-dependent effects, the full unseparated shredded material is also relevant for practical application. In our parallel work, the as-received mechanically shredded WTB fiber was directly incorporated into mortar at 0.5, 1, and 2 vol% and showed potential as a fiber-type recycled addition [31]. At the same time, we recognize that fractionation may generate a very fine powder fraction. Rather than treating this fraction as residual waste, our other work also investigates its use as a partial cement replacement at levels up to 15 wt%, which may provide an additional valorization route while contributing more directly to clinker reduction [5].

5. Conclusions

This study utilizes different sizes of wind turbine blade (WTB) waste as fiber reinforcement in mortar to investigate the alkali-silica reaction (ASR) expansion and the durability of the composite matrices. The results show that WTB size strongly affects both the mechanical response and the ASR behavior of the mortar. Larger WTB fractions (>8 mm), which more often retained epoxy resin on the surface, showed lower early ASR expansion, likely because the resin layer limited direct exposure of the glass phase and the larger fragments provided some restraint against early expansion. However, these coarse fractions also introduced more defects and higher porosity, which negatively affected compressive strength. The results indicate that the practical challenge is not to treat WTB waste as a conventional reinforcing material, but to identify the size ranges and incorporation conditions under which this waste can be accommodated in cementitious mixtures without causing unacceptable detrimental effects. The following detailed conclusions can be drawn:

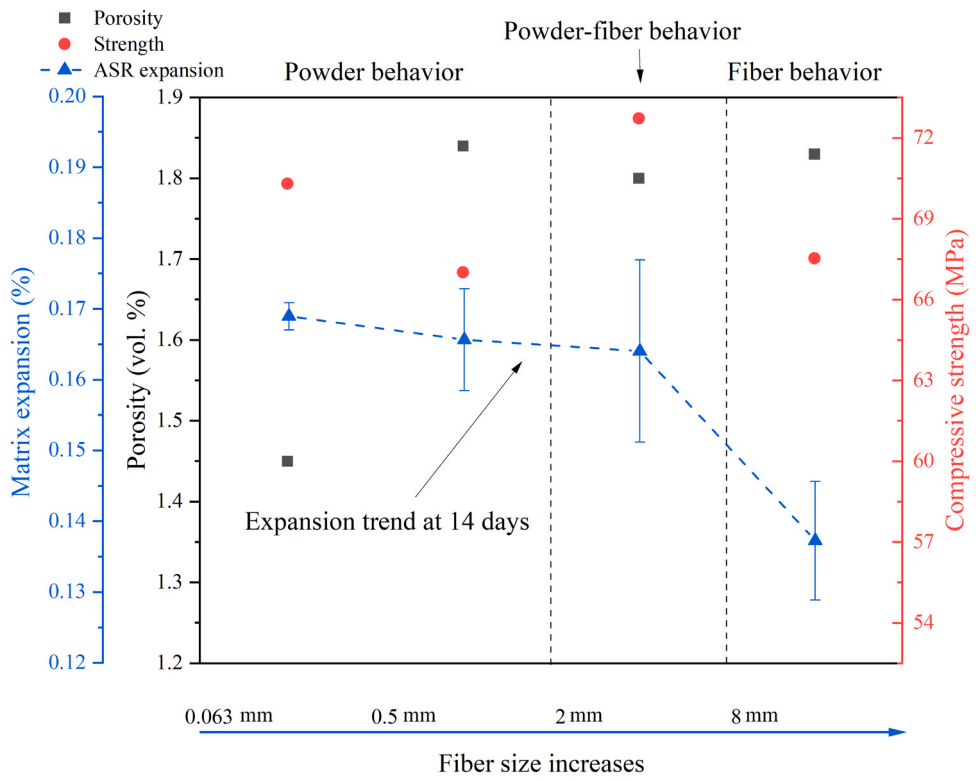

Fig. 21. Effect of WTB waste fiber size on strength and ASR.

- The WTB waste shows the activity and different dissolution rates under a varying alkaline environment. The increased pH environment promotes the dissolution of exposed glass fiber leading to additional release of Ca^{2+}, Mg^{2+}, $Si(OH)_4$, and $Al(OH)_4^-$ ions into an alkaline solution. This will promote the formation of C(N)-A-S-H gels and $Mg(OH)_2$.
- Smaller WTB waste fibers undergo a more intensive shredding process, leading to greater exposure of glass fibers and increased dissolution of Ca^{2+} ions due to extensive interaction with the alkaline solution. SEM images show that smaller fibers lose their round shape under alkali attack. Conversely, larger WTB fibers have more epoxy resin encapsulating the glass fibers, reducing their exposure to the alkaline solution and resulting in lower Ca^{2+} ion dissolution.
- As fiber size increases, both the Ca atomic ratio range and the height of the hydration peak decrease. Smaller WTB waste fibers have a higher Ca atomic ratio in formed gels due to their greater surface area and more exposed glass fibers, leading to more extensive calcium ion dissolution. This higher dissolution rate consumes more OH^- ions early in the hydration process, with the exposed epoxy resin also consuming OH^- ions, resulting in decreased heat release and a delayed hydration reaction, lowering the peak height. Conversely, larger WTB fibers, with epoxy encapsulating the glass fibers, exhibit less calcium ion dissolution and OH^- ion consumption, leading to a higher hydration reaction and peak height.
- WTB waste fiber size influences both mortar performance and durability, and this risk is strongly governed by the size-dependent morphology of the waste, particularly the balance between exposed glass fibers and resin-covered surfaces. The finer fractions (0.063–2 mm) improved compressive strength and reduced porosity, but also caused higher ASR expansion, showing that better mechanical performance does not necessarily mean better durability. The medium fraction (2–8 mm) showed an intermediate response, while the coarsest fraction (>8 mm) introduced more defects and increased porosity. The ASR results further indicate that finer fractions (W0.063 and W0.5) led to faster expansion, whereas coarser fractions (W2 and W8) showed delayed but still significant expansion. These findings highlight that WTB waste in cementitious materials must be evaluated not only by strength, but also by ASR-related durability, since larger particle size does not necessarily reduce expansion risk.

The future application of shredded WTB waste in cementitious materials is differentiated by the fiber size. Small WTB waste fibers (0.063–2 mm) are recommended for use as SCMs, while larger WTB waste fibers (>8 mm) are recommended for use as fiber reinforcement. There is a limitation that fresh density and occluded air content were not measured in the present experimental program. These parameters are relevant to the interpretation of pore structure and hardened performance and should therefore be included in future investigations.

CRediT authorship contribution statement

De Souza Diego Jesus: Writing – review & editing, Methodology, Investigation. **Wolfgang Kunther:** Writing – review & editing, Supervision. **Ana Teresa Lima:** Writing – review & editing, Supervision, Resources, Project administration, Funding acquisition. **Tao Liu:** Writing – original draft, Validation, Methodology, Investigation, Formal analysis, Data curation, Conceptualization. **Charilaos Paraskevoulakos:** Writing – review & editing, Methodology, Investigation, Formal analysis.

Declaration of Competing Interest

The authors declare that they have no known competing financial interests or personal relationships that could have appeared to influence the work reported in this paper.

Acknowledgments

This work was supported by the European Union's Horizon Europe Research and Innovation Programme under grant agreement no.

101096437 funded by the European Union. Views and opinions expressed are however those of the author(s) only and do not necessarily reflect those of the European Union or the European Climate, Infrastructure and Environment Executive Agency (CINEA). Neither the European Union nor the granting authority can be held responsible. During the preparation of this work, the authors used ChatGPT in order to improve readability, grammar, and language. After using this tool/service, the authors reviewed and edited the content as needed and took full responsibility for the content of the publication.

Appendix A. Supporting information

Supplementary data associated with this article can be found in the online version at doi:10.1016/j.conbuildmat.2026.146416.

Data availability

Data will be made available on request.

References

[1] D.Y.C. Leung, Y. Yang, Wind energy development and its environmental impact: a review, Renew. Sustain. Energy Rev. 16 (2012) 1031–1039, https://doi.org/10.1016/j.rser.2011.09.024.
[2] A. Tyurkay, G.M. Kirkelund, A.T.M. Lima, State-of-the-art circular economy practices for end-of-life wind turbine blades for use in the construction industry, Sustain. Prod. Consum 47 (2024) 17–36, https://doi.org/10.1016/j.spc.2024.03.018.
[3] G.T. Xu, M.J. Liu, Y. Xiang, B. Fu, Valorization of macro fibers recycled from decommissioned turbine blades as discrete reinforcement in concrete, J. Clean. Prod. 379 (2022), https://doi.org/10.1016/j.jclepro.2022.134550.
[4] T. Liu, C. Paraskevoulakos, U.A. Mughal, A. Tyurkay, N. Lushnikova, H. Song, C. Duyal, S.T. Karnick, F. Gauvin, A.T. Lima, Mechanisms and applications of wind turbine blade waste in cementitious composites: a review, Mater. Des. (2025) 113732, https://doi.org/10.1016/j.matdes.2025.113732.
[5] T. Liu, C. Duyal, C. Paraskevoulakos, K. Enemark-Rasmussen, A. Tyurkay, N. Lushnikova, F. Gauvin, A.T. Lima, Effect of wind turbine blade waste on cement hydration and gel structure: Competitive interaction of glass and polyester resin, Compos. B Eng. 311 (2026) 113273, https://doi.org/10.1016/j.compositesb.2025.113273.
[6] C. Duyal, M. Chevalier, N. Lushnikova, F. Gauvin, H.J.H. Brouwers, Optimized incorporation of shredded wind turbine blade waste in concrete using a particle packing approach, Constr. Build. Mater. 521 (2026) 146102, https://doi.org/10.1016/j.conbuildmat.2026.146102.
[7] D. Baturkin, O.A. Hisseine, R. Masmoudi, A. Tagnit-Hamou, L. Massicotte, Valorization of recycled FRP materials from wind turbine blades in concrete, Resour. Conserv. Recycl 174 (2021) 105807, https://doi.org/10.1016/j.resconrec.2021.105807.
[8] S. Yousef, J. Eimontas, I. Stasiulaitiene, K. Zakarauskas, N. Striūgas, Recovery of energy and carbon fibre from wind turbine blades waste (carbon fibre/unsaturated polyester resin) using pyrolysis process and its life-cycle assessment, Environ. Res. 245 (2024) 118016, https://doi.org/10.1016/j.envres.2023.118016.
[9] C. Paraskevoulakos, T. Liu, A.T. Lima, Investigating the microstructure of mortar systems reinforced with wind turbine blade waste using X-ray computed tomography, Constr. Build. Mater. 509 (2026) 145187, https://doi.org/10.1016/j.conbuildmat.2026.145187.
[10] V. Revilla-Cuesta, M. Skaf, V. Ortega-López, J.M. Manso, Raw-crushed wind-turbine blade: Waste characterization and suitability for use in concrete production, Resour. Conserv. Recycl 198 (2023) 107160, https://doi.org/10.1016/j.resconrec.2023.107160.
[11] V. Revilla-Cuesta, J. Manso-Morato, N. Hurtado-Alonso, M. Skaf, V. Ortega-López, Mechanical and environmental advantages of the revaluation of raw-crushed wind-turbine blades as a concrete component, J. Build. Eng. 82 (2024) 108383, https://doi.org/10.1016/j.jobe.2023.108383.
[12] T. Liu, C. Paraskevoulakos, A.T. Lima, 2024, Mitigation of Alkali-Silica Reaction by Shredded Wind Turbine Blade Waste in Mortar, in: : pp. 504–514. https://doi.org/10.1007/978-3-031-62690-6_52202450451410.1007/978-3-031-62690-6_52.
[13] J. Lindgård, Ö. Andiç-Çakır, I. Fernandes, T.F. Rønning, M.D.A. Thomas, Alkali–silica reactions (ASR): Literature review on parameters influencing laboratory performance testing, Cem. Concr. Res. 42 (2012) 223–243, https://doi.org/10.1016/j.cemconres.2011.10.004.
[14] L.F.M. Sanchez, B. Fournier, M. Jolin, J. Duchesne, Reliable quantification of AAR damage through assessment of the Damage Rating Index (DRI), Cem. Concr. Res. 67 (2015) 74–92, https://doi.org/10.1016/j.cemconres.2014.08.002.
[15] L.F.M. Sanchez, B. Fournier, M. Jolin, D. Mitchell, J. Bastien, Overall assessment of Alkali-Aggregate Reaction (AAR) in concretes presenting different strengths and incorporating a wide range of reactive aggregate types and natures, Cem. Concr. Res. 93 (2017) 17–31, https://doi.org/10.1016/j.cemconres.2016.12.001.
[16] B. Fournier, M.-A. Bérubé, Alkali-aggregate reaction in concrete: a review of basic concepts and engineering implications, Can. J. Civ. Eng. 27 (2000) 167–191, https://doi.org/10.1139/cjce-27-2-167.
[17] F. Rajabipour, E. Giannini, C. Dunant, J.H. Ideker, M.D.A. Thomas, Alkali–silica reaction: Current understanding of the reaction mechanisms and the knowledge gaps, Cem. Concr. Res. 76 (2015) 130–146, https://doi.org/10.1016/j.cemconres.2015.05.024.
[18] S.H. Diab, A.M. Soliman, M.R. Nokken, Feasibility of basalt and glass FRP mesh for strengthening and confinement concrete damage due to ASR-expansion, Constr. Build. Mater. 266 (2021) 120893, https://doi.org/10.1016/j.conbuildmat.2020.120893.
[19] H. Yazıcı, The effect of steel micro-fibers on ASR expansion and mechanical properties of mortars, Constr. Build. Mater. 30 (2012) 607–615, https://doi.org/10.1016/j.conbuildmat.2011.12.051.
[20] G. Jen, R. Hay, C.P. Ostertag, Multi-scale evaluation of hybrid fiber restraint of alkali-silica reaction expansion in concrete, Constr. Build. Mater. 211 (2019) 1117–1126, https://doi.org/10.1016/j.conbuildmat.2019.03.102.
[21] M. Iorio, F. Marra, M.L. Santarelli, J. González-Benito, Reinforcement-matrix interactions and their consequences on the mechanical behavior of basalt fibers-cement composites, Constr. Build. Mater. 309 (2021) 125103, https://doi.org/10.1016/j.conbuildmat.2021.125103.
[22] C. Lin, T. Kanstad, S. Jacobsen, G. Ji, Bonding property between fiber and cementitious matrix: A critical review, Constr. Build. Mater. 378 (2023) 131169, https://doi.org/10.1016/j.conbuildmat.2023.131169.
[23] H. Song, T. Liu, F. Gauvin, H.J.H. Brouwers, Improving the interface compatibility and mechanical performances of the cementitious composites by low-cost alkyl ketene dimer modified fibers, Constr. Build. Mater. 395 (2023) 132186, https://doi.org/10.1016/j.conbuildmat.2023.132186.
[24] L. Ge, X. Li, H. Feng, C. Xu, Y. Lu, B. Chen, D. Li, C. Xu, Analysis of the pyrolysis process, kinetics and products of the base components of waste wind turbine blades (epoxy resin and carbon fiber), J. Anal. Appl. Pyrolysis 170 (2023) 105919, https://doi.org/10.1016/j.jaap.2023.105919.
[25] L. Ge, C. Xu, H. Feng, H. Jiang, X. Li, Y. Lu, Z. Sun, Y. Wang, C. Xu, Study on isothermal pyrolysis and product characteristics of basic components of waste wind turbine blades, J. Anal. Appl. Pyrolysis 171 (2023) 105964, https://doi.org/10.1016/j.jaap.2023.105964.
[26] Y. Tao, S.A. Hadigheh, Y. Wei, Recycling of glass fibre reinforced polymer (GFRP) composite wastes in concrete: A critical review and cost benefit analysis, Structures 53 (2023) 1540–1556, https://doi.org/10.1016/j.istruc.2023.05.018.
[27] B. Benmokrane, M. Hassan, M. Robert, P.V. Vijay, A. Manalo, Effect of Different Constituent Fiber, Resin, and Sizing Combinations on Alkaline Resistance of Basalt, Carbon, and Glass FRP Bars, J. Compos. Constr. 24 (2020), https://doi.org/10.1061/(ASCE)CC.1943-5614.0001009.
[28] C. Shi, Y. Wu, C. Riefler, H. Wang, Characteristics and pozzolanic reactivity of glass powders, Cem. Concr. Res. 35 (2005) 987–993, https://doi.org/10.1016/j.cemconres.2004.05.015.
[29] W.L. Lam, Y. Cai, K. Sun, P. Shen, C.S. Poon, Roles of ultra-fine waste glass powder in early hydration of Portland cement: Hydration kinetics, mechanical performance, and microstructure, Constr. Build. Mater. 415 (2024) 135042, https://doi.org/10.1016/j.conbuildmat.2024.135042.
[30] H. Heng, F. Meng, J. McKechnie, Wind turbine blade wastes and the environmental impacts in Canada, Waste Manag. 133 (2021) 59–70, https://doi.org/10.1016/j.wasman.2021.07.032.
[31] T. Liu, H. Reascos, U.A. Mughal, G.M. Kirkelund, A.T. Lima, Improving mortar properties with waste wind turbine blade fibers and superplasticizer, Constr. Build. Mater. 472 (2025) 140864, https://doi.org/10.1016/j.conbuildmat.2025.140864.
[32] ASTM C1260, 2007, ASTM C1260, Standard Test Method for Potential Alkali Reactivity of Aggregates (Mortar-Bar Method) 1, . www.astm.org,2007⟨www.astm.org⟩.
[33] EU, Fibres for concrete - Part 1: Steel fibres - Definitions, specifications and conformity, EN 14889-1: 2006 (2009). .
[34] I. Nikolić, A. Drinčić, D. Djurović, L. Karanović, V.V. Radmilović, V.R. Radmilović, Kinetics of electric arc furnace slag leaching in alkaline solutions, Constr. Build. Mater. 108 (2016) 1–9, https://doi.org/10.1016/j.conbuildmat.2016.01.038.
[35] ASTM C1897-20 Standard Test Methods for Measuring the Reactivity of Supplementary Cementitious Materials by Isothermal Calorimetry and Bound Water Measurements, 2020. .
[36] EN 196-1:2016 Methods of testing cement - Part 1: Determination of strength, (2016).
[37] D.V. Okhrimenko, S.H.Q. Barly, M. Jensen, L.Z. Lakshtanov, D.B. Johansson, M. Solvang, Y.Z. Yue, S.L.S. Stipp, Surface evolution of aluminosilicate glass fibers during dissolution: Influence of pH, solid-to-solution ratio and organic treatment, J. Colloid Interface Sci. 606 (2022) 1983–1997, https://doi.org/10.1016/j.jcis.2021.09.148.
[38] T. Liu, S. Li, Y. Chen, H.J.H. Brouwers, Q. Yu, In-situ formation of layered double hydroxides in MgO–NaAlO2-activated GGBS / MSWI BA: Impact of Mg2+ on reaction mechanism and leaching behavior, Cem. Concr. Compos 140 (2023) 105114, https://doi.org/10.1016/j.cemconcomp.2023.105114.
[39] T. Mi, E.-H. Yang, C. Unluer, Passivation of reinforcing steel in reactive MgO cement blended with Portland cement, Cem. Concr. Compos 143 (2023) 105269, https://doi.org/10.1016/j.cemconcomp.2023.105269.
[40] L. Rodier, V. da Costa Correia, H. Savastano Junior, Elaboration of eco-efficient vegetable fibers reinforced cement-based composites using glass powder residue, Cem. Concr. Compos 110 (2020) 103599, https://doi.org/10.1016/j.cemconcomp.2020.103599.

[41] B. Yuan, Q.L. Yu, H.J.H. Brouwers, Evaluation of slag characteristics on the reaction kinetics and mechanical properties of Na 2 CO 3 activated slag, Constr. Build. Mater. 131 (2017) 334–346, https://doi.org/10.1016/j.conbuildmat.2016.11.074.
[42] T. Liu, Q. Yu, H.J.H. Brouwers, X. Fan, Utilization of waste glass in alkali activated slag/fly ash blends: reaction process, microstructure, and chloride diffusion behavior, J. Sustain. Cem. Based Mater. 12 (2023) 516–526, https://doi.org/10.1080/21650373.2022.2082577.
[43] D. Hernández Fraile, E. Faccin, F. Minelli, G. Plizzari, A. Muttoni, Fibre orientation in SFRC slabs and consequences for punching shear and flexural resistance, Eng. Struct. 302 (2024) 117364, https://doi.org/10.1016/j.engstruct.2023.117364.
[44] V. Revilla-Cuesta, A.B. Espinosa, F. Fiol, R. Serrano-López, M. Skaf, Exploring the behavior of concrete containing selectively crushed wind-turbine blade from a water-transport perspective, Case Stud. Constr. Mater. 22 (2025) e04821, https://doi.org/10.1016/j.cscm.2025.e04821.